IEEE Access
Multidisciplinary | Rapid Review | Open Access Journal

Received May 19, 2022, accepted June 2, 2022, date of publication June 16, 2022, date of current version June 24, 2022.

Digital Object Identifier 10.1109/ACCESS.2022.3183968

Biosignal Monitoring Clothing System for the Acquisition of ECG and Respiratory Signals

SHUENN-YUH LEE[1], (Senior Member, IEEE), YI-WEN HUNG[1], (Student Member, IEEE), PO-HAN SU[1], (Graduate Student Member, IEEE), I-PEI LEE[2], AND JU-YI CHEN[3]

[1]Department of Electrical Engineering, National Cheng Kung University, Tainan City 70101, Taiwan
[2]School of Medicine, Kaohsiung Medical University, Kaohsiung 807378, Taiwan
[3]Department of Internal Medicine, National Cheng Kung University Hospital, College of Medicine, National Cheng Kung University, Tainan 70101, Taiwan

Corresponding authors: Shuenn-Yuh Lee (ieesyl@mail.ncku.edu.tw) and Ju-Yi Chen (juyi@mail.ncku.edu.tw)

This work was supported in part by the Taiwan Semiconductor Research Institute and the Ministry of Science and Technology (MOST), Taiwan, under Grant MOST 110-2218-E-006-015.

ABSTRACT The detection of biosignals by using a comfortable material is important to improve human health. This paper presents a complete wearable system with smart clothing for the long-term monitoring of lead-I ECG and respiratory signals. The proposed system is divided into three parts, including biosignal-monitoring clothing, a biosignal acquisition device, and a software platform. The smart clothing integrates fabric-based ECG dry electrodes, conductive fiber traces, and a high-sensitivity capacitive respiration transducer to sense the biosignals. The challenge including the integration of ECG electrodes and the respiration transducer in the clothing system to provide the high-quality ECG and respiration signals for clinical use has been overcome in the proposed biosignal-monitoring clothing. The sensed signals on the smart clothing are collected in the biosignal-acquisition device through fabric-based traces and a specially designed clothing structure. Furthermore, the biosignals are processed using the biosignal-acquisition device and sent to the remote smart device through the Bluetooth module. The device according to the requirement of the front-end clothing system and the actual measurement accuracy is implemented and contributed onto the reduction in the effect of motion artifact. The software platform on the smart device provides real-time biosignal monitoring and health-information analysis. A highly efficient ECG QRS complex detection algorithm and respiratory-rate detection algorithm are also proposed. The ECG QRS complex detection algorithm is verified using the MIT/BIH Arrhythmia Database to demonstrate the achievement of high performance. The overall measured sensitivity, positive prediction, and error rate of the proposed algorithm are 99.86%, 99.93%, and 0.19%, respectively. The measured ECG signal of the clothing system is compared with the commercial silver/silver-chloride electrode by using the BIOPAC MP36 acquisition system. The result confirms the high quality of the signal, so the measured ECG signal can be used for medical applications. The function of the respiration transducer is verified by the BIOPAC SS11LA airflow transducer, and the overall accuracy of 19 test subjects is 98.74%. Using the proposed system, long-term health care in daily life can be achieved.

INDEX TERMS Biosignal acquisition, smart clothing, respiratory signal, electrocardiogram, QRS complex detection, wearable device.

I. INTRODUCTION

Population aging is a worldwide trend. World Health Organization has reported that world's population aged 60 years is up to 900 million in 2015, which is expected to reach 2 billion by 2050 [1]. The changing age profile of the population has increased the importance of health care, and biosignal monitoring technology plays an important role in the development of the health care system. Biosignal monitoring technology is used to detect body signals. By analyzing the collected signals, relevant health information of the object can be obtained, and appropriate disposition or medical action can be taken.

Using a wearable system is a convenient way to achieve such a technology. The combination of wearable devices and biosignal monitoring technology may provide long-term,

The associate editor coordinating the review of this manuscript and approving it for publication was Sung-Min Park.

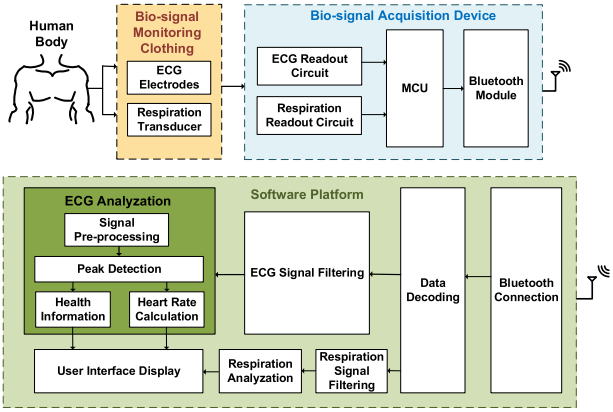

FIGURE 1. Block diagram of the proposed smart clothing system.

FIGURE 2. Appearance of the biosignal monitoring clothing. (a) External appearance. (b) Internal appearance.

location-independent measurement of biosignals. Among all applications of wearable systems, smart clothing is the most important. Smart clothing is a biosignal monitoring system based on clothing, and it has some advantages among the other wearable systems. First, unlike most wearable devices, such as watch devices and belt, clothing is necessary for everyone in daily life; therefore, related wearable devices can be easily accepted by users. In addition, smart clothing can provide a large variety of biosignal monitoring compared with other wearable systems because it has a large area contacting to the body surface of the user. For instance, vital signs such as electrocardiogram (ECG) signal and respiration rate can be measured by wearing smart clothing on the chest and abdomen, respectively. ECG signal is the tiny electrical activity caused by the diastole and systole of cardiac muscle. The acquisition of ECG signal can provide health information such as heart rate. Moreover, using the morphology of ECG signal is a common way to diagnose heart diseases such as arrhythmia [2]. The respiratory rate is the frequency of respiration behavior, which consists of an inhalation cycle and exhalation cycle. The normal respiration rate for an adult at rest is 12 to 20 breaths per minute, and sickness, fever, and other serious clinical diseases can be detected by monitoring the abnormal respiratory rate [3], [4].

The ECG signal and respiratory rate can be observed in several ways. In measuring the ECG signal, electrodes are placed on patient's limbs and on the surface of the chest [5], [6] to collect the tiny electrical signals generated by heart contraction and based on different angles. Silver/silver-chloride (Ag/AgCl) electrode (wet electrode) is commonly used in ECG signal detection. The wet gel of the electrode is highly compatible with the human surface; therefore, it provides high-quality signal in the biosignal acquisition system. However, the characteristics of the electrolytic conductive gel may cause allergy or discomfort under prolonged contact. In addition, the gelatinous material will dry out under long-term biosignal measurement, which limits the use of long-term health care. Thus, a dry electrode is an alternative approach. Dry electrodes, such as non-contact [7], [8] or conductive [9] fabric-based electrodes, can provide long-term biosignal measurement. Rachim *et al.* [8] integrated a fabric-based dry electrode into an armband to monitor the ECG signal and obtained the information of heart rate. Myers *et al.* [9] presented a silver nanowire-based dry electrode and combined the electrodes into a hand ring to measure electromyography and ECG signals. Baek *et al.* [10] tested a polymeric dry electrode for long-time wear and demonstrated the good fidelity of the dry electrode in a 7-day experiment. All these previous works [7]–[10] have demonstrated the validity of dry electrodes for ECG signal monitoring. For respiratory rate detection, the method can be primarily categorized into two groups. The first group of methods are observing the airflow during breathing. This group of methods have high accuracy for monitoring the respiratory rate. However, they are inconvenient for long-term monitoring and difficult to be integrated into the wearable devices. The other group of methods are estimating the respiration rate based on the movement of the body surface. For example, Kundu *et al.* proposed a capacitive detection method to detect the respiratory rate [11]. Two electrodes are fixed on the inner anterior and posterior sides of the clothing, and the human body is embedded in the middle serving as a dielectric to form a capacitance structure transducer. The respiration rate can be conveniently obtained by this method, and the structure is suitable to achieve smart clothing.

Numerous clothing systems with biosignal monitoring have been reported in recent years. Boehm *et al.* [12], [13] developed a 12-lead ECG T-shirt. The conductive electrodes are sewn in specific positions to acquire multichannel ECG signals. Rienzo *et al.* [14] showed the single-lead ECG signal, seismocardiogram (SCG), and other vital signs with a clothing system to assess cardiac mechanical performance during sleep in microgravity. Koyama *et al.* [15] designed a clothing system with a novel smart textile incorporating stable single-mode transmission heterocore optical-fiber sensor. The clothing system detects the vibration generated by heartbeat and respiration behavior. Bu *et al.* [16] proposed a single-lead ECG monitoring garment and inferred respiratory

TABLE 1. Literature review with recent biosignal-monitoring clothing systems.

Clothing System	Provided Biosignals	Advantages and Disadvantages
12-Lead ECG T-shirt [12][13]	12-Lead ECG	**Pros**: multichannel ECG, test in different activities **Cons**: conductive trace is not fibrillated, morphology of ECG signal is affected
Garment for assessing cardiac mechanical performance [14]	Single-lead ECG, SCG, respiratory rate, and skin temperature	**Pros**: various biosignal monitoring, indexes of cardiac mechanic are provided **Cons**: limited to a static measurement environment
Smart textile using heterocore optical fiber for biosignal monitoring [15]	Heartbeat and respiratory rate	**Pros**: novel noncontact biosignal monitoring **Cons**: low accuracy, sensitive to motion artifact
ECG monitoring garment with silver-coated electrodes [16]	Single-lead ECG and respiratory rate	**Pros**: washable, easy to mass produce, complete validation for general applications **Cons**: lack of clinical validation, low accuracy in respiratory-rate detection

rate from the measured ECG signal. The clothing system provides some validation such as washing durability test of the dry electrodes for practical use in daily life. The features, advantages, and disadvantages of this clothing system are listed in Table 1.

This study proposes a complete smart clothing system containing a biosignal-monitoring clothing, a biosignal-acquisition device, and a software platform to provide long-term wireless monitoring and analysis of lead-I ECG and respiratory signals. Compared with [12], the proposed ECG electrodes, respiration transducer, and conductive traces are all fabric based, and the high integration is beneficial for wearable contact with comfortable condition. The lead-I ECG position provides more information for rhythm reading than that of the nonstandard position, such as the monitoring systems proposed in [8], [14], and [16]. The high-quality ECG signals measured in our proposed clothing system have been approved compared with the measured system by using Ag/AgCl electrodes. Moreover, the proposed capacitive structure of the respiration transducer allows the use of the smaller area than a previous work [11] and can be easily integrated into the clothing along with the conductive textile traces and ECG-sensing electrodes. The high sensitivity of the transducer can provide a more accurate respiratory rate than that in [16]. A highly efficient real-time ECG QRS complex detection method and a respiratory-rate detection algorithm are also achieved on the software platform of a remote smart device to calculate the heart rate and respiration rate, respectively. Therefore, health information such as energy expenditure (EE) and heart-rate variability (HRV) can be acquired.

II. MATERIALS AND METHODS

Figure 1 shows the proposed biological signal monitoring clothing system for the monitoring of lead-I ECG and respiratory signals. The system primarily contains three components, including biosignal monitoring clothing, a biosignal acquisition device, and a software platform on the remote smart device. The biosignal monitoring clothing acquires the ECG and respiratory signals using the ECG electrodes and respiration transducer, respectively. The biosignal acquisition device processes the sensed signal and converts the signal into digital data, which are wirelessly transmitted to a remote smart device by a Bluetooth 5.2 module. The software platform on the remote smart device then displays the real-time biosignal data waveform after receiving data and further analyzes the data based on the proposed algorithms. A highly efficient QRS peak detection algorithm is proposed and applied to ECG data analysis to acquire the desired health information. Moreover, a proposed peak detection algorithm is used in respiration data processing to calculate the respiration rate.

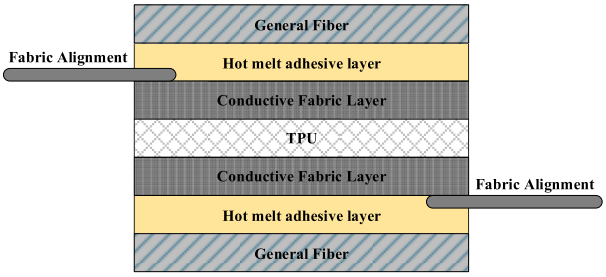

FIGURE 3. Fabric structure of the respiration transducer.

A. BIOSIGNAL MONITORING CLOTHING

An overview of the biosignal monitoring clothing is shown in Fig. 2. The ECG electrodes on the clothing are used to detect the small voltage change on the body surface caused by cardiac muscle depolarization. The design of the ECG electrodes is a protruding structure with the size of 6.2 cm × 5.6 cm × 0.5 cm, which is filled with a soft elastomeric material and covered with a conductive fabric. Therefore, the ECG electrodes can touch the body surface tightly during the activity of the user to avoid motion artifact (MA) on the ECG signal. The position of the ECG electrodes is designed on the basis of the lead-I placement of the Mason–Likar modification of standard 12 lead [17]. The Mason–Likar monitoring position is widely used in modified electrode placement [18]. The placement provides good stability of the ECG recording [19]. Furthermore, the tightening strap is stitched on the external front side of the clothing,

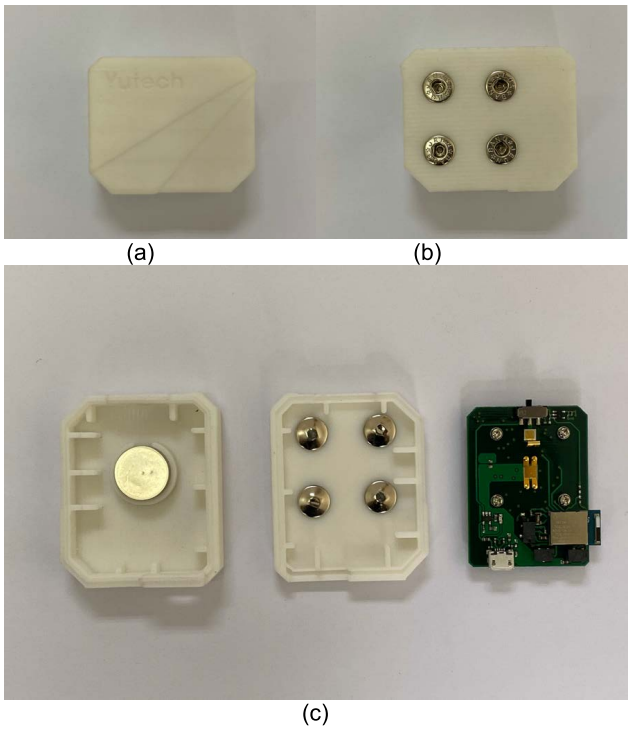

FIGURE 4. Package of the biosignal acquisition device. (a) Front view of the device. (b) Back view of the device. (c) Interior view of the device and PCB of the biosignal acquisition device.

pressing the ECG electrodes on the body surface to improve the ECG signal quality.

The respiration transducer is placed on the inner anterior side of the clothing and implemented using a multi-layered architecture (Fig. 3). The transducer primarily contains two conductive fabric layers and an intermediate dielectric material layer to form a capacitive structure, and the respiration behavior can be detected on the basis of the change in the capacitance value. The proposed work adopts a 0.05 mm thermoplastic polyurethane (TPU) as the dielectric material, which provides several advantages. First, the high elasticity of TPU enables the transducer to provide a more significant rate of change in capacitance to the pressure applied by the body surface; therefore, the difficulty of detecting the respiration behavior is reduced. Second, TPU has sufficient relative permittivity, and it can be implemented in a thin dielectric layer. Hence, the transducer can provide a large initial capacitance value with a small area, and it can be integrated with ECG electrodes and associated traces in the limited available area of the smart clothing system. Furthermore, the thin dielectric layer reduces the thickness of the transducer, thereby increasing the wearing comfort of the clothing. The size of the respiration transducer in its current design is 13.5 cm $\times$ 4.2 cm $\times$ 0.05 cm, and the capacitance value is approximately several nanofarads (nF). In the inhalation cycle of the respiration behavior, the lung expands and causes the peritoneal cavity to press the respiration transducer. The thickness of the intermediate dielectric material layer will be decreased to increase the capacitance value of the transducer.

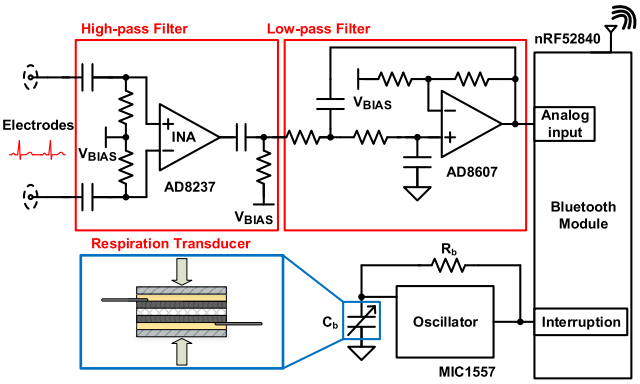

FIGURE 5. Schematic of two channels for measuring ECG and respiratory signals.

By contrast, in the exhalation cycle, the lung contracts, and the pressure to the transducer will decrease. Thus, the thickness of the intermediate dielectric material layer is increased, and the capacitance value of the transducer is decreased. With the observation of the capacitance value, the complete cycles of respiration, including the inhalation and exhalation cycles, can be detected.

Based on the above-mentioned signal acquisition methods from ECG electrodes and respiration transducer, the signals are delivered out from the ECG electrodes and respiration transducer via conductive traces, and the nickel-plated brass buttons on the end of the traces is used to link signal transmission between the internal and external side of the clothing. In addition, these buttons are used together with biosignal acquisition device in the pocket to gather the delivered signals and fasten the device on the external side of the clothing.

B. BIOSIGNAL ACQUISITION DEVICE

The biosignal acquisition device shown in Fig. 4 primarily integrates an ECG signal acquisition circuit, a respiratory signal acquisition circuit, and a microcontroller using a Bluetooth 5.2 module (nRF52840). A Bluetooth 5.2 module is acceptable for most mobile devices, providing sufficient transmission speed and consuming less power than WI-FI. Moreover, the security of Bluetooth is high. Hence, a Bluetooth 5.2 module is selected in our system to achieve wireless transmission.

In this work, the ECG signal is measured using two dry electrodes, which serve as signal electrodes. The reference electrode and drive-right-leg electrode are not used to maximize the wearing comfort. Moreover, the effect of half-cell potential of the electrode–tissue interface should be noted. With these considerations, an AC-coupled front-end composed of a high-pass filter and low-pass filter is adopted in the ECG channel, as shown in the upper part of Fig. 5. The ECG signal is initially filtered with a high-pass filter, and an instrumentation amplifier (AD8237) is utilized to provide gain and convert the differential signal to single-ended signal. Moreover, a second-order low-pass filter is designed using an amplifier (AD8607) to attenuate the high-frequency noise and serve as a post-amplifier.

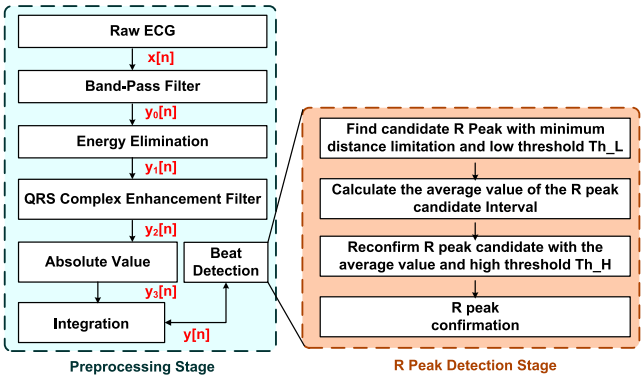

FIGURE 6. Block diagram of the processing steps using the QRS complex detection algorithm.

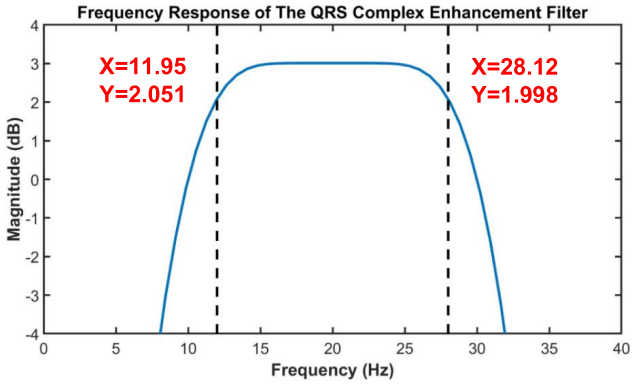

FIGURE 7. Frequency response of the QRS complex enhancement filter.

The frequency band of the ECG signal in clinical practice is between 0.05 and 100 Hz [20]. Therefore, the corner frequency of the high-pass filter and low-pass filter in this study is designed to be 0.03 and 155 Hz, respectively. In addition, considering that the amplitude of ECG is in the range of approximately 0.5–4 mV [21], [22], the measured gain in the ECG channel is set to approximately 55 dB to overcome MA and match with the requirement of ADC [22] behind the amplifier. In the proposed system with power of 3.3 V, the voltage range is kept at the above-mentioned gain because the ECG signals measured using dry electrodes can be affected by MA. The output of the ECG channel is digitized by a 12-bit ADC built in the nRF52840 with sampling frequency of 400 Hz, and the processed data are wirelessly transmitted to a remote smart device for further analysis.

An oscillator (MIC1557) and the feedback resistance are adopted to convert the capacitance variation into frequency change and record the status of the respiration transducer, as shown in the lower part of Fig. 5. When the user first puts on the proposed clothing, the initial capacitance of the transducer is recorded as C_b. The pressure applied to the transducer may vary depending on user's body type; therefore, C_b is not a fixed value. The movement of the body surface during respiration may cause the capacitance of the transducer to vary from C_b to $C_b + \Delta C_b$, and the oscillation frequency will change from f to $f + \Delta f$. The relationship

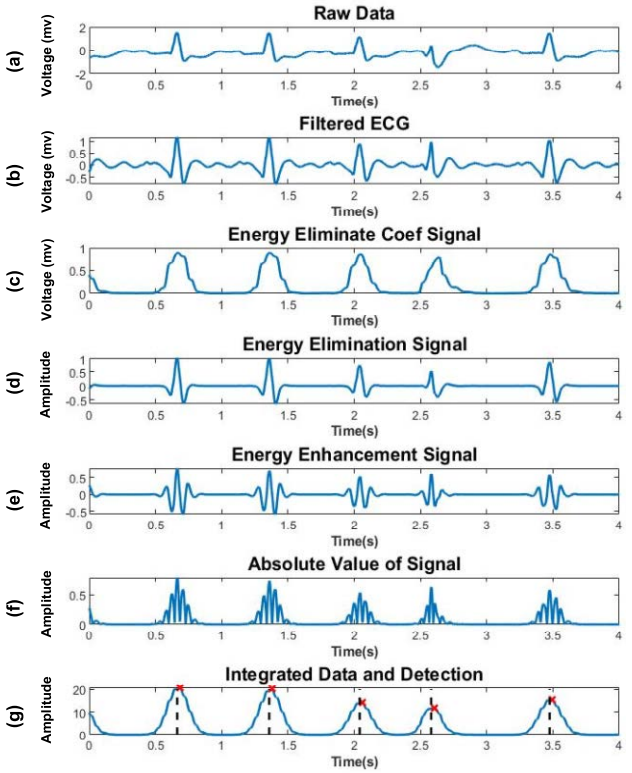

FIGURE 8. Processing results of ECG QRS complex feature generation and peak detection results from MIT-BIH database record 109. (a) ECG raw data, x[n]. (b) Filtered ECG output, $y_0[n]$. (c) Coefficient data, coef[n], for energy elimination. (d) Energy elimination data, $y_1[n] = y_0[n]$ x coef[n]. (e) Energy enhancement data, $y_2[n]$. (f) Absolute value, $y_3[n]$. (g) Blue line: Integrated Data y[n]. Black dashed line: Golden location of the QRS complex peak. Red cross point: Detection peak of the ECG QRS complex.

between Δf and ΔC_b is derived in (1).

$$\Delta f = \frac{-\Delta C_b}{k_1 R_b (C_b + C_p)(C_b + \Delta C_b + C_p)}. \tag{1}$$

In this equation, k_1 is a constant regarding the performance of the oscillator. R_b represents the feedback resistance, and C_p denotes the parasitic capacitance of the transducer. Considering that the variation ΔC_b and C_p are smaller than C_b in the proposed transducer, the corresponding change in frequency Δf can be simplified as follows (2):

$$\Delta f = \frac{-\Delta C_b}{k_1 R_b C_b^2}. \tag{2}$$

Given the high elasticity of TPU, the variation ΔC_b is sensitive to the movement of the body surface. Hence, the respiration behavior can be simply observed by Δf. A counter is programed in the nRF52840 to record the oscillation frequency. Every rising edge of the oscillator output triggers the counter to increase based on the interruption command. After counting for a specific period of time, the count is wirelessly transmitted to the remote smart device, and the counter is reset for the next cycle. Therefore, the value of the counter is proportional to the oscillation frequency. In addition, the longer the calculation period for the counter,

the higher the resolution of the oscillation frequency variation. However, the increased Bluetooth data transfer rate may increase the power consumption and difficulty of Bluetooth transmission. Consequently, the measured sampling period in the respiration channel is selected to be 12.5 ms, which is five times higher than that of the ECG channel. In this study, the resolution of the oscillation frequency variation is 80 Hz, and the size of the counter is 12 bits.

C. SOFTWARE PLATFORM

The software platform on the remote smart device provides biosignal analysis, including ECG QRS complex detection, respiratory rate detection, HRV calculation, and EE estimation after receiving the data. The procedure of the QRS complex detection algorithm is divided into the preprocessing stage and R peak detection stage (Fig. 6). The preprocessing stage is primarily divided into five steps, as shown on the left side of Fig. 6. The ECG signal often suffers from MA and high-frequency noise [23], and the main frequency component of the QRS complex is 5 Hz to 22 Hz [24]. Thus, the raw ECG signal x[n] is first filtered by a third-order elliptic band-pass filter with a frequency range of 5–50 Hz to remove the MA and high-frequency noise, and the filtered ECG signal is denoted as y_0[n]. Furthermore, the in-band noise is removed using energy elimination [25]. The coefficient data are created using a long sliding window and a short sliding window, as shown in equation (3).

$$Coef(n) = \frac{\sum_{k=n-w\_s}^{k=n+w\_s} y_0[k]^2}{\sum_{k=n-w\_l}^{k=n+w\_l} y_0[k]^2}, \tag{3}$$

where $y_0[k]$ represents the filtered ECG data, and w_s and w_l denote the half of the short sliding window size and long sliding window size, respectively. The short sliding window is used to capture the energy of the ECG QRS complex; therefore, the width of the short sliding window is set to be slightly larger than the width of the common QRS complex width, which is 150 ms [26]. In addition, the duration of the long sliding window is set to 1 s to calculate the energy of the desired region. In this work, the filtered ECG data is selected rather than the ECG raw data for calculation to prevent the large variation of the magnitude of the coefficient data caused by the ECG baseline drift. The denoised ECG signal y_1[n] is obtained by multiplying the coefficient data by the filtered ECG signal y_0[n]. Next, the wavelet function is utilized to emphasize the location of the ECG QRS complex. The decomposition high-pass filter of Daubechies wavelets [27] is selected because of its similarity to the shape of the ECG QRS complex. Eight zeros are interpolated into the coefficients of the filter to form a QRS complex enhancement filter. Adding zeros can emphasize the location of the QRS complex without reinforcing the location of the noise. The wavelet order is decided according to the signal-to-noise ratio (SNR) comparison in Table 2. An impulse is passed through the QRS complex enhancement filter designed with a different wavelet to determine the different SNR values of the filtered signal.

TABLE 2. Performance comparison between different mother wavelet for the QRS complex enhancement filter.

Selected Mother Wavelet	SNR (dB)
Haar	0.6645
Daubechies 2	1.0672
Daubechies 3	1.2157
Daubechies 4	**1.2950**
Daubechies 5	1.3460
Daubechies 6	1.3822
Coiflets 3	1.0813

The frequency band of the QRS wave between 5 Hz to 22 Hz [24] is defined as the signal band. This SNR value helps us observe the enhancement ability of the QRS complex and the degree of decay for the remaining frequency component that may cause false-positive detection. Most Daubechies wavelets have a good SNR value and is suitable to design the enhancement filter. The difference in the SNR value between Daubechies 3, Daubechies 4, Daubechies 5, and Daubechies 6 is tiny because they are similar in morphology. However, with increased order of wavelets, the computational load is also raised. Therefore, Daubechies 4 is appropriately used to design the QRS enhanced filter in this work, and the frequency response of the QRS complex enhancement filter is shown in Fig. 7. The signal is amplified in the 12 Hz to 28 Hz band, which overlaps with the main frequency component of the ECG QRS complex. Based on the convolution of the denoised ECG signal y_1[n] with the coefficient of the enhancement filter, the location of the QRS complex can be emphasized, and the output signal is denoted as y_2[n]. The energy of y_2[n] is simply evaluated by taking the absolute value (4). Then, an integration moving window, which is 150 ms long, is applied point by point to y_3[n] to capture the energy of the QRS complex and generate the data y[n] for the next R peak detection stage. The calculation of y[n] is shown in equation (5), where w indicates the half length of the integration moving window.

$$y_3[n] = \text{abs}(y_2[n]) \tag{4}$$

$$y[n] = \sum_{k=n-w}^{k=n+w} y_3[k]. \tag{5}$$

The right side of Fig. 6 shows the flow of the peak detection stage. Two amplitude thresholds, Th_H and Th_L, are used to locate the R peak position. The R peak candidates, R′ [n], are first determined from the peaks of the integration waveform y[n] with a low amplitude threshold Th_L and the minimum distance limitation between each R peak candidate. Th_L is set to 8.5, and the minimum distance limitation is set to 250 ms on the basis of the maximum heart rate for a normal person [28]. Once the R peak candidates are decided, the average of the eight continuous intervals of the R peak candidate is calculated using equations (6) and (7).

$$RR'[n] = R'[n] - R'[n-1]. \tag{6}$$

$$RR'_{mean}[n] = \frac{RR'[n-7] + RR'[n-6] + \cdots RR'[n]}{8}. \tag{7}$$

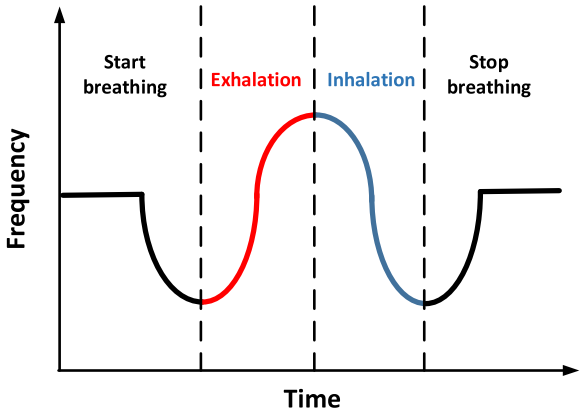

FIGURE 9. Schematic waveform diagram of the respiratory signal generated from the frequency variation of the oscillator.

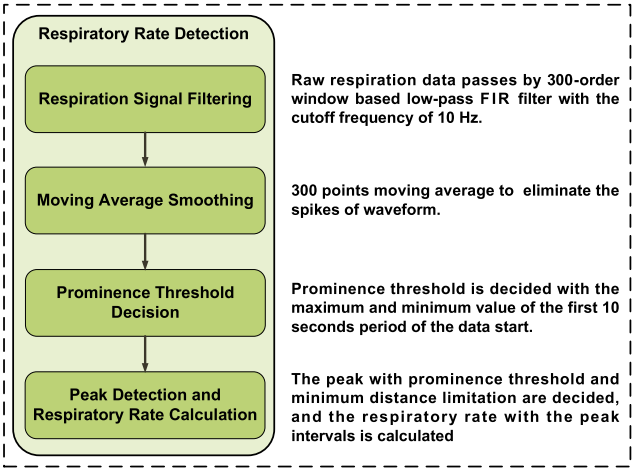

FIGURE 10. Processing steps of the respiratory rate detection algorithm.

If the latest interval of the continuous interval $RR'[n]$ is less than 1.1 times of RR'_{mean}[n], then the high amplitude threshold Th_H is applied to the latest R peak candidate $R'[n]$. If the amplitude of $R'[n]$ is smaller than Th_H, which is set to 1, then the R peak candidate $R'[n]$ is removed. Based on the proposed method, the location of the remaining R peak candidates can be regarded as the location of the R peaks. Fig. 8 uses the ECG segment of the MIT-BIH database [29] record 109 to illustrate the step-by-step output results of the preprocessing stage and the detection results of the proposed QRS complex detection algorithm. Using the time interval among the R peaks, the heart rate can be calculated. Moreover, HRV can be acquired using the variation in the continuous time interval of more than 5 min [30]. Furthermore, EE during submaximal exercise can be predicted by the calculated heart rate using the additional information, including age, gender, and weight [31].

The schematic waveform diagram of the respiratory signal generated from the frequency variation of the oscillator is illustrated in Fig. 9. The rising stage of the waveform represents the exhalation behavior, whereas the falling stage indicates the inhalation behavior. Finding the positive peaks of the waveform, which indicates the time point when the exhalation phase changes to the inhalation phase, is one method of detecting the respiratory rate. On the basis of this method, the respiratory rate detection algorithm is proposed (Fig. 10). The raw respiration data are first processed by a 300-order window-based low-pass finite impulse response (FIR) filter with a cutoff frequency of 10 Hz to eliminate the high-frequency noise. The cutoff frequency of the FIR filter is selected on the basis of the normal respiration rate of less than 30 times per minute. Moreover, a 300-point moving average is applied to the signal to smooth the waveform, and the waveform output is denoted as r[n]. After the pre-processing steps, r[n] is used in a peak detection method to find the positive peak. However, the baseline of r[n] may be affected by the body type of the user and the size of the smart clothing. Moreover, the tight contact surface between the respiration transducer and body surface leads to a high baseline value of the respiratory signal. Therefore, the prominence of the peak is used instead of the value to distinguish noise peak from the desired positive peak. The value of the prominence threshold is decided on the basis of individual data. The maximum value and minimum value of the first 10 s from the starting point of the data will be recorded, and the prominence threshold is calculated by equation (8).

$$MinPeakProminence = \frac{Data\_Max - Data\_Min}{8} \tag{8}$$

In addition, the minimum distance limitation for each positive peak is added for peak detection. Consequently, the peak of r[n], which falls more than the value of the prominence threshold and more than 0.4 s from the previous positive peak, will be considered as the desired positive peak. The respiratory rate can be calculated using the interval between each positive peak position.

III. EXPERIMENT RESULTS

A. VALIDATION OF DRY ELECTRODES AND CONDUCTIVE FIBER TRACE PERFORMANCE FOR ECG

The effect of the impedance of the dry electrodes and conductive fiber traces on the ECG signal quality was first investigated. In this experiment, a CONTEC MS400 multi-parameter simulator was used as the ideal ECG source to eliminate the surface effect on the human body [32]. The BIOPAC MP36 four-channel data acquisition system [33] provided high-quality ECG signal monitoring, and the BIOPAC SS2LB lead set [34] was used as the connection wire. The direct-contact ECG waveform was measured by connecting the output of the MS400 simulator to the BIOPAC MP36 acquisition system. The measured waveform is shown in the orange line in Fig. 11(a). In addition, the dry electrodes were connected to the output of the MS400 simulator to receive the ECG signal and measure the ECG signal affected by the impedance of the dry electrodes and conductive fiber traces. Then, the nickel-plated brass buttons on the smart clothing were connected to the BIOPAC MP36 acquisition system through BIOPAC SS2LB wire. Therefore, the ECG signal transmission path contained the dry electrodes and

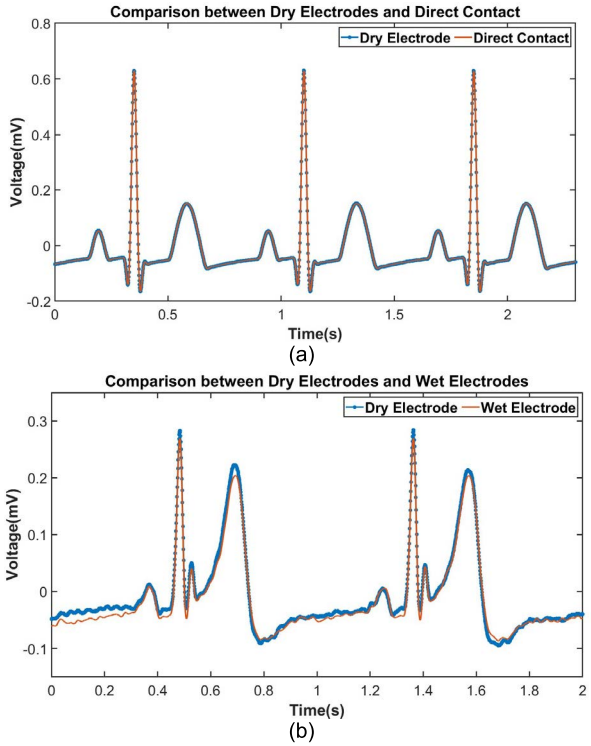

FIGURE 11. Performance verification of dry electrodes and conductive fiber traces. (a) Direct contact to ideal ECG signal source. (b) Actual measurement from the human body.

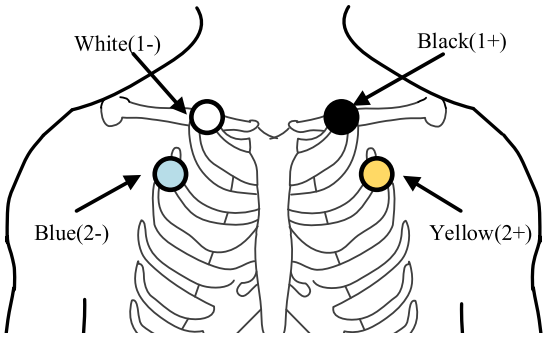

FIGURE 12. Lead-I electrode placement suggested by Holter monitor [6] (white circle and black circle) and the electrode placement in the proposed system (blue circle and yellow circle).

total conductive fiber traces of ECG signal on the smart clothing. The measured waveform is illustrated in blue asterisk line in Fig. 11(a). The experiment showed that two waves were similar, and the tiny non-ideal effects caused by the impedance of the dry electrodes and conductive fiber traces were the same as the SS2LB lead set. Moreover, the result showed high efficiency of ECG transmission architecture on the smart clothing.

The compatibility of the electrode material with the biological surface may affect the quality of the ECG signal. Hence, the effect of the ECG signal quality caused by the skin-electrode impedance of the dry electrodes was also studied. The test subject wore the smart clothing to monitor the lead-I ECG signal using the first sensing channel of the

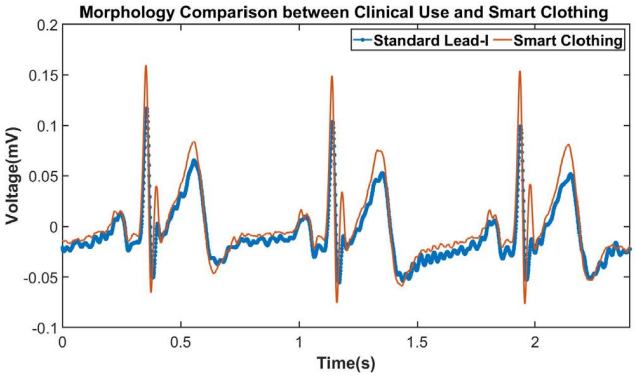

FIGURE 13. Shape comparison between the clinical standard lead-I ECG and the signal measured by the proposed system.

BIOPAC MP36 acquisition system. The measured signal is shown in blue asterisk line in Fig. 11(b). The two locations, where the dry electrodes on the smart clothing contacted with the skin, were recorded as A and B, which were denoted as 2− and 2+ in Fig. 12, respectively. In addition, two commercial silver/silver-chloride electrodes (wet electrodes) were placed as close to A and B as possible to measure the same ECG signal as the second sensing channel of the BIOPAC MP36 acquisition system. The measured signal is shown in the orange line in Fig. 11(b). The result showed that the ECG signal measured by the dry electrodes is similar to that detected by the wet electrodes, and the non-ideal effect caused by the dry electrodes in the proposed system can be neglected.

B. COMPARISON OF ECG SIGNAL MEASURED BY THE PROPOSED SYSTEM AND STANDARD LEAD-I ECG MEASURED SYSTEM

Considering the signal quality and clothing production, the position of electrodes in the proposed system differs from the standard electrode position used by a Holter monitor [6], and the difference in the placement of electrodes will affect the shape of the ECG signal. Moreover, the difference in characteristics between dry and wet electrodes affects the quality of the ECG signal. Therefore, in this section, the ECG signal measured in the smart clothing is compared to the standard lead-I ECG measured system in clinical trial. Two commercial wet electrodes were placed on the left-mid-clavicular and right-mid-clavicular of the test subject to measure the standard lead-I ECG signal at the position suggested by the Holter monitor, and the measured ECG signal was collected by the first sensing channel of the BIOPAC MP36 acquisition system. In addition, the test subject wore the smart clothing to monitor the ECG signal using the second sensing channel of the BIOPAC MP36 acquisition system. The detailed placement of the electrodes in this experiment is shown in Fig. 12, and the measured result is shown in Fig. 13. The polarity of the P wave, QRS complex, and T wave of the ECG signal measured by the proposed system are similar to those of the ECG signal measured at standard lead-I

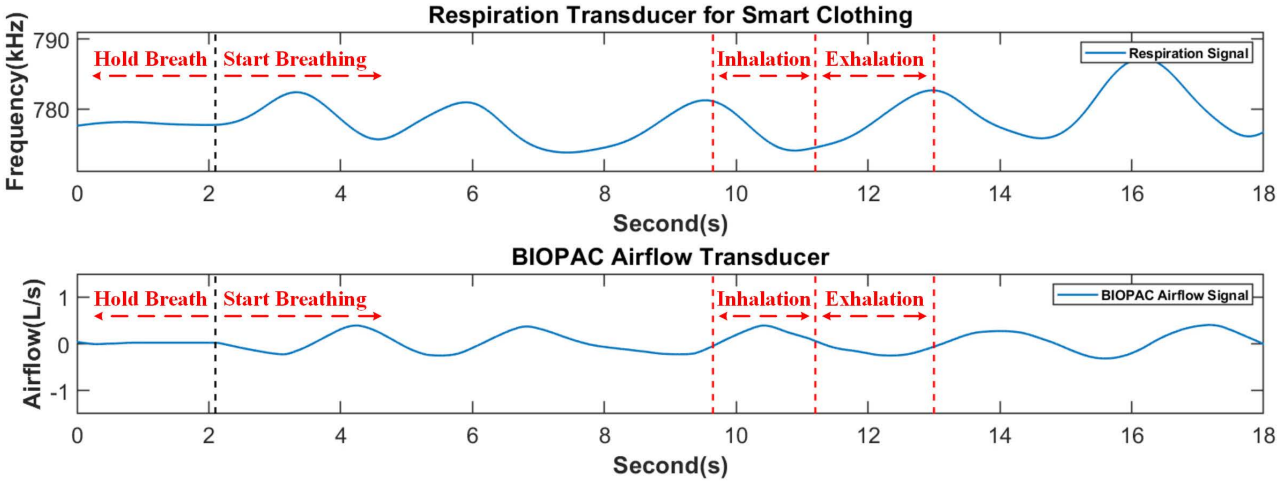

FIGURE 14. Comparison of measured waveform of respiratory signals using the BIOPAC system and respiration transducer of smart clothing.

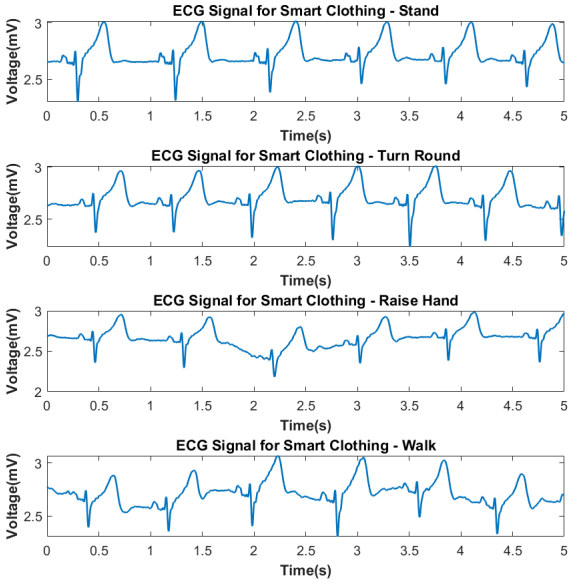

FIGURE 15. ECG signal measurement of proposed clothing during different activities.

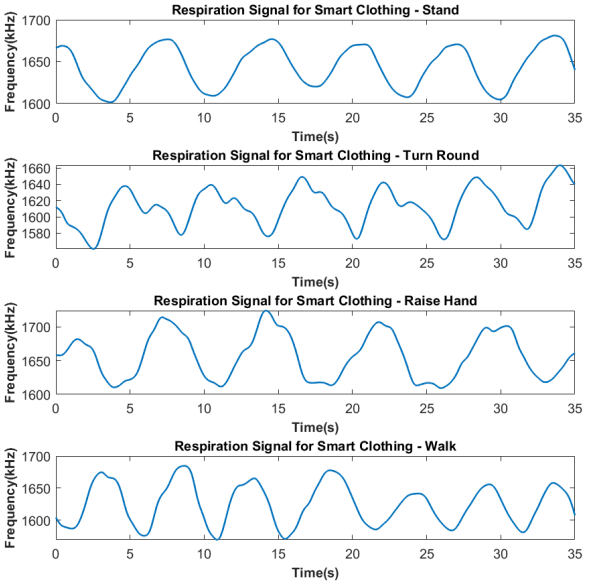

FIGURE 16. Respiratory signal measurement of proposed clothing during different activities.

position with wet electrodes, and the correlation in time interval among them remains unchanged. Consequently, common arrhythmias such as premature ventricular contraction can be further identified behind the proposed system.

C. RESPIRATION TRANSDUCER FUNCTION VALIDATION

The function of the respiration transducer was validated by the BIOPAC SS11LA airflow transducer [35]. The SS11LA airflow transducer provided airflow and lung volume monitoring for human, which could directly observe the respiration behavior. Nineteen test subjects, including 12 males and seven females, were approached to test the performance. Each test subject wore the smart clothing and held the SS11LA airflow transducer in the mouth. Using the respiration transducer integrated into the smart clothing and airflow transducer, the movement of the body surface of the subjects and the respiratory airflow caused by the respiration behavior were monitored simultaneously. The breathing of subjects was restricted by a nose clip to breathe through the mouth and ensure airflow in and out through the mouth, and the subjects stayed motionless during the whole experimental procedure. In addition, the subjects were asked to perform specific breathing behavior to align the timing of the two different monitoring systems, including the BIOPAC system and the proposed biosignal acquisition device. First, the subjects were asked to hold their breath for a while. Then, the subjects began to breathe freely, and the time point between stop breathing and free breathing of each subject was marked as the benchmark of the common start point of the breathing. After breathing for a specified period, the subjects stopped breathing, and the time point

between free breathing and stop breathing of each subject was noted as the benchmark of the common end point of the breathing. The whole experiment was fixed for 10 min. The partial measurement waveforms of one of the subjects are shown in Fig. 14. The measurement waveform on the top was obtained by the proposed biosignal acquisition system, and the waveform in the bottom was achieved by the BIOPAC system. The correlation between the two different monitoring systems was evaluated by comparing the number of breaths between the starting and ending points of the two waveforms for each subject. The respiration time of the waveform of the BIOPAC system was denoted as the compared golden reference. The less respiration time of the proposed biosignal acquisition system was regarded as the miss detection, and the number of times missing was recorded as the number of false-negative (FN) detection. The extra respiration time of the proposed biosignal acquisition system was regarded as the error detection, and the number of extra detections was denoted as the false-positive detection (FP). According to equation (9), the average accuracy of the proposed respiration system was 98.74%.

$$Accuracy\,(\%) = \frac{TP}{TP + FP + FN} \times 100\%. \tag{9}$$

D. BIOSIGNAL MONITORING OF THE PROPOSED CLOTHING FOR DIFFERENT ACTIVITIES

The signal quality of the biosignal monitoring clothing has been tested in different activities. The ECG and respiratory signal measurement results are shown in Figs. 15 and 16, respectively. The same subject performed the activities of standing, continuous back and forth rotation of the upper body (turn round), continuous hand-ups and hand-downs (raise hand) and walking, and the subject also wore the proposed clothing to monitor the biosignals. The ECG signals (Fig. 15) measured in standing and continuous back and forth rotation of the upper body showed good quality with little baseline shift. The ECG signals measured in continuous hand-ups and hand-downs and walking suffer from slight baseline drift. However, most of the P waves, QRS complexes, and T waves of the ECG signal can be clearly identified. For the respiration measurement (Fig. 16), the respiration waveforms in all activities except for continuous back and forth rotation of the upper body were clear. The waveform in the activity of the rotation of the upper body suffers from slight signal interference because of the friction between the respiration transducer and the body surface during the movement but without affecting the identification of the respiration rate.

E. BENCHMARKING STUDY OF THE QRS COMPLEX DETECTION ALGORITHM USING THE MIT-BIH ARRHYTHMIA DATABASE

The performance of the algorithm was evaluated by the MIT-BIH arrhythmia database [29]. The MIT-BIH arrhythmia database contains 48 excerpts of ambulatory ECG, which are sampled at 360 Hz. In addition, it contains part of arrhythmias, which are also disturbed by noise during record. Consequently, it is a benchmark database to test the strength of our proposed algorithms. The total database, except for part of the record 207, which is unannotated [39], was analyzed using the proposed QRS complex detection algorithm. The performances, including sensitivity (Se), positive prediction (P+), and error rate (ERR), were calculated using the following equations:

$$Se\,(\%) = \frac{TP}{TP + FN} \times 100\%, \tag{10}$$

$$P_+\,(\%) = \frac{TP}{TP + FP} \times 100\%, \tag{11}$$

$$ERR\,(\%) = \frac{FP + FN}{TP + FP + FN} \times 100\%. \tag{12}$$

where TP indicates true-positive detection; FP indicates false-positive detection, and FN indicates false-negative detection. The analysis result of each record is illustrated in Table 3, and the total Se, P+, and ERR are 99.86%, 99.93%, and 0.19%, respectively. Performance comparison among the proposed methods, the well-known Pan–Tompkins algorithm [36], and other recent QRS complex detection algorithms [25], [37]–[42] is presented in Table 4. The proposed algorithm revealed similar or slightly better performance than most of the state-of-the-art algorithms. In particular, it performed well in P+. The convolutional recurrent neural network (CRNN) model proposed by Cai *et al.* [41] had the best performance. However, the high computation of the proposed algorithm hindered its implementation on mobile device. By contrast, the proposed QRS complex detection algorithm had low complexity, and it can be easily implemented on mobile device for real-time analysis.

F. REAL-TIME MONITORING SOFTWARE INTERFACE

The software interface was implemented on mobile device with an iOS platform, and the measured results, including ECG and respiratory signals, are shown in Fig. 17(a). The application was uploaded on a public platform (named:YuCloth). The first channel presets the display of lead-I ECG waveform, and the second channel is default to show the filtered respiration passed by the low-pass filter with cutoff frequency of 3 Hz. The display content of each channel can be adjusted. The ECG and respiratory signals were immediately analyzed by the previously proposed algorithms to calculate the heart rate and respiration rate, respectively, and display in the list at the bottom of the software interface. Health information, such as EE and HRV, is shown in Fig. 17(b).

IV. DISCUSSION

In this work, a complete smart clothing system, which provides the monitoring of lead-I ECG and respiratory signals, is proposed. The ECG electrodes and respiration transducer are integrated into the clothing to monitor the target biosignal. The conductive fabric-based ECG electrodes have a protruding structure with the size of 17.36 cm^3. The respiration

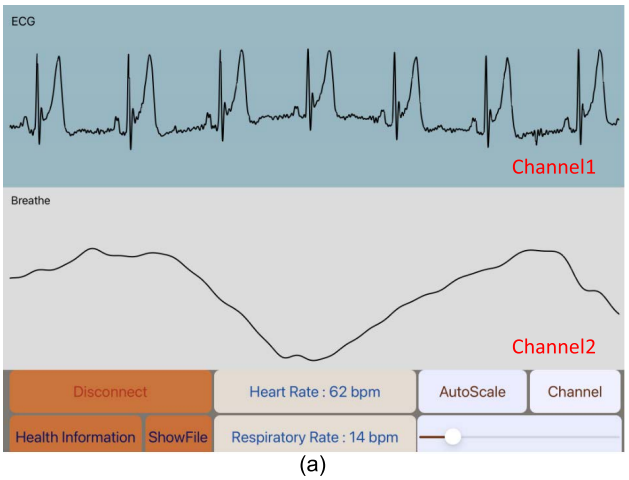

(a)

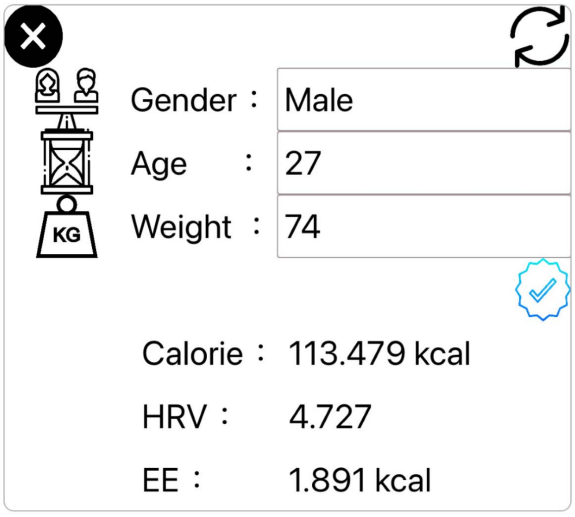

(b)

FIGURE 17. Real-time monitoring software interface on iOS device. (a) Main display interface. (b) Health information interface.

transducer is primarily composed of two conductive fabric layers and a highly elastic TPU with a 0.05 mm intermediate dielectric material layer to form a capacitive structure under a smaller sensing area. In this work, the issue of long-term use of smart clothing is considered. For example, the hot-melt adhesive layer improves the durability and stability of the respiration transducer in daily use. However, it may reduce sensitivity. According to the sample test, for the capacitance value change when applying pressure to the transducer, the change rate of the transducer with a hot-melt adhesive layer is about 1/3 times that of the transducer without a hot-melt adhesive layer. Although the change of capacitance is reduced by the hot-melt adhesive layer, the result is still sufficient for the respiratory rate detection. Thus, the hot-melt adhesive layer is embedded in the structure of the proposed respiration transducer in the smart clothing.

The effect of MA should also be overcome when implementing the biosignal monitoring clothing. Loose ECG electrode contact will cause the skin-electrode impedance to drastically change during the object movement, and the variation may cause the baseline drift or saturation of the ECG signal. Strengthening the tightness of clothing to prevent electrode slippage can solve this problem. Nevertheless, excessively tight clothing might cause the dielectric material of the respiration transducer close to the compression limit, which may reduce detection sensitivity. Moreover, it will cause measurement discomfort for the user. Therefore, the tightness of the clothing should be carefully designed to meet the above-mentioned requirements.

The biosignal acquisition device with a supply voltage of 3.3 V primarily includes an ECG signal acquisition circuit, respiratory signal acquisition circuit, and microcontroller with a Bluetooth 5.2 module. The ECG signal acquisition

TABLE 3. Result of the proposed ECG QRS complex detection algorithm using the MIT-BIH arrhythmia database.

Record No.	TP	FP	FN	P+ (%)	Se (%)	ERR (%)
100	2271	0	0	100	100	0
101	1864	3	0	99.84	100	0.16
102	2185	0	0	100	100	0
103	2083	0	0	100	100	0
104	2224	5	3	99.78	99.97	0.36
105	2561	22	10	99.15	99.61	1.23
106	2027	1	0	99.95	100	0.05
107	2136	0	0	100	100	0
108	1759	2	3	99.89	99.83	0.28
109	2530	0	0	100	100	0
111	2122	0	1	100	99.95	0.05
112	2537	0	0	100	100	0
113	1793	0	0	100	100	0
114	1875	0	4	100	99.79	0.21
115	1951	0	0	100	100	0
116	2395	0	16	100	99.34	0.66
117	1533	0	0	100	100	0
118	2277	0	0	100	100	0
119	1987	0	0	100	100	0
121	1860	0	1	100	99.95	0.05
122	2474	0	0	100	100	0
123	1517	0	0	100	100	0
124	1618	0	0	100	100	0
200	2598	0	2	100	99.92	0.08
201	1953	0	8	100	99.59	0.41
202	2133	0	2	100	99.92	0.08
203	2934	0	45	100	98.49	1.51
205	2654	0	1	100	99.96	0.04
207	1855	0	4	100	99.78	0.22
208	2940	0	13	100	99.56	0.44
209	3003	1	0	99.97	100	0.03
210	2638	0	10	100	99.62	0.38
212	2747	0	0	100	100	0
213	3248	0	1	100	99.97	0.03
214	2258	0	2	100	99.91	0.09
215	3360	0	1	100	99.97	0.03
217	2207	0	1	100	99.95	0.05
219	2154	0	0	100	100	0
220	2046	0	0	100	100	0
221	2423	0	3	100	99.88	0.12
222	2474	0	7	100	99.72	0.28
223	2604	0	0	100	100	0
228	2051	14	1	99.32	99.95	0.73
230	2254	0	0	100	100	0
231	1569	12	0	99.24	100	0.76
232	1780	9	0	99.50	100	0.50
233	3076	0	1	100	99.97	0.03
234	2752	0	0	100	100	0
Total	**109430**	**69**	**140**	**99.93**	**99.86**	**0.19**

TABLE 4. Performance comparison between recent QRS complex detection systems and methods.

Method	Se (%)	P+ (%)	ERR(%)
Pan-Tompkins algorithm [36]	99.76	99.56	0.68
Yazdani *et al.* (2016) [25]	99.87	99.86	0.28
Chen *et al.* (2017) [37]	99.82	99.81	0.36
Hou *et al.* (2018) [38]	99.32	99.45	1.23
Sharma *et al.* (2019) [39]	99.89	99.83	0.29
Lee *et al.* (2019) [40]	99.82	99.90	0.28
Cai *et al.* (2020) [41]	**99.94**	**99.97**	**0.09**
Malik *et al.* (2020) [42]	99.92	99.62	-
Proposed algorithm	**99.86**	**99.93**	**0.19**

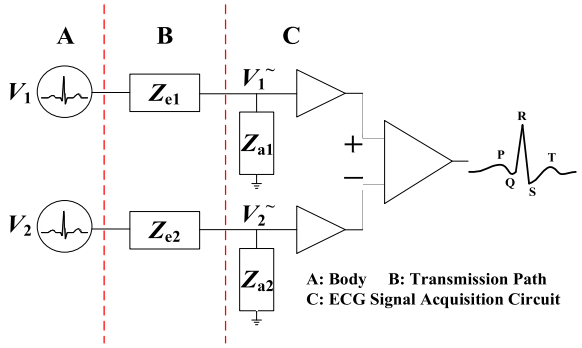

FIGURE 18. ECG signal measurement environment.

circuit has an AC-coupled front-end composed of a high-pass filter and low-pass filter with a frequency range between 0.03 Hz and 155 Hz, and the gain is approximately 55 dB. The measured output of the ECG channel is digitized by a 12-bit ADC built in the nRF52840 with a sampling frequency of 400 Hz. An oscillator (MIC1557) is adopted to convert the capacitance variation of the respiration transducer into frequency change. The counter of the nRF52840 is used to sample the output of the MIC1557 for 12.5 ms. The resolution of the frequency change is 80 Hz. The digitized biosignals are transmitted to the remote smart device through a Bluetooth 5.2 module and analyzed using the proposed algorithms.

The software platform is implemented on mobile device with an iOS platform to receive the data and provide real-time biosignal display, heart rate, respiration rate, and health information, such as EE and HRV. The heart rate and respiration rate are calculated using the proposed algorithms. The proposed QRS complex detection algorithm for heart rate acquisition is verified by the MIT-BIH database, and the number of total failed detection beats for the MIT-BIH arrhythmia database is 209. The total sample points of the ECG database are denoted as n points, and the sampling rate is 360 Hz. The total computational load for n-point ECG signal is approximately 491n additions, 436n multiplications, n divisions, and 5n comparisons, and the time complexity is O(n). Part of the coefficient data calculation in equation (3) accounts for the majority of all operations. With regard to the space complexity of the proposed real-time QRS detection algorithm, the storage of processed ECG data and the filter coefficients account for the most use of space. The coefficient number of the IIR filter and proposed QRS complex enhancement filter is quite low. The size of the storage data should be at least 1 s larger than the size of the long sliding window. Therefore, the size of the storage can be several seconds long. The proposed QRS complex detection algorithm was implemented on Matlab R2019, and the related software program has been released in GitHub [43]. The performance testing was executed in the environment capable of hardware configuration of 2.8 GHz Intel core i5 CPU with 16 GB RAM. The average execution time for the half-hour single record in the MIT-BIH arrhythmia database is 0.157 s. For the well-known Pan–Tompkins algorithm [36], the number of total failed detection beats for the MIT-BIH arrhythmia database is 784. The average execution time was calculated using the open public code [44] and tested under the same environment. Analysis of the half-hour single record in the MIT-BIH arrhythmia database is completed within 0.224 s. The proposed QRS complex detection algorithm and Pan–Tompkins algorithm have the same complexity. However, the number of total failed detection beats of the proposed QRS detection complex algorithm is only about one-third of that of the Pan–Tompkins algorithm. In addition, although the accuracy of CRNN QRS detection algorithm [41] is slightly better than that of the proposed QRS complex detection algorithm, the execution time is also about several hundred times longer. Hence, the proposed QRS complex detection algorithm is capable of higher efficiency. Moreover, the ECG QRS detection algorithm can be the foundation of heart disease classification. The widely used strategy to classify heart diseases is beat-by-beat analysis [45]. ECG signals are often divided into the input segments of the convolutional neural network based on the location of R peak and heart rate [46], [47]. Moreover, RR interval is often selected to be the features for other classifier such as support vector machine [48], [49] because the rhythm information of the heartbeat is often used clinically as a basis for diagnosis of arrhythmias.

The proposed respiration rate detection algorithm primarily uses 306n additions, 302n multiplications, and 4n comparisons for the n points respiration data, and the time complexity is O(n). The 300-order FIR filter in the algorithm accounts for most of the computation. For the moving average method in the algorithm, the computation can be simplified. By recording the first moving average result, subsequent moving average calculations only need to add the latest data and deduct the oldest data. In addition, the concept of the circular queue can reduce the computation load for moving average. For the part of space complexity, the 300-order FIR filter can be designed to be coefficient symmetric; therefore, the storage of the coefficient can be reduced to 151 floating-point data. The remaining part is primarily the 300 points for storage of respiration raw data and 300 points circular queue for calculating the moving average operation. Therefore, approximately 751 points of floating-point data storage space will be used for the computation of real-time respiration rate.

The performance of the smart clothing system for ECG signal acquisition is tested in several ways in this paper. The

effect of the impedance of the dry electrodes and conductive fiber traces on the signal quality was first tested, and the result is shown in Fig. 11(a), showing the high efficiency of ECG transmission architecture on the smart clothing. Afterward, the performance of the dry electrode is compared with that of the commercial silver/silver chloride electrode. The result in Fig. 11(b) shows that the shape of ECG signals between the monitoring system with proposed dry electrodes and that with wet electrodes is similar. Therefore, high-quality ECG signal can be provided using the proposed dry electrodes. The impact of the skin-electrode interface on ECG signal [50] can be investigated to improve the signal quality of ECG signal with dry electrodes. The large impedance of the skin-electrode interface can lead to the degradation of measured ECG signal. The ECG signal measurement environment is shown in Fig. 18. Part A is the body. V_1 and V_2 are the voltages of the positive and negative terminals of the source ECG signal, respectively, and the source ECG signal in equation (13) is the real ECG signal that has not been affected by the impedance of the transmission path. Part B is the complete path of the signal transmission. In the proposed system, the source ECG signal is initially sensed by electrode, and it is transmitted to the ECG signal acquisition circuit through the conductive path on the clothing. Z_{e1} and Z_{e2} are the impedance on the transmission path. Part C is the ECG signal acquisition circuit. Z_{a1} and Z_{a2} are the input impedance of the amplifier. $V_1^{\sim}$ and $V_2^{\sim}$ are the actual voltages at the input of the amplifier, and the actual measured ECG signal is shown in equation (14). If Z_{e1} is equal to Z_{e2}, and Z_{a1} is equal to Z_{a2}, then the relationship between the source ECG signal and the actual measured ECG signal can be derived using equation (15).

$$ECG_{src} = V_1 - V_2, \tag{13}$$

$$ECG_{meas} = V_1^{\sim} - V_2^{\sim}, \tag{14}$$

$$\text{If } Z_{a1} = Z_{a2} = Z_{a2}, \quad Z_{e1} = Z_{e2} = Z_e,$$

$$ECG_{meas} = ECG_{src} \times \frac{Za}{(Za + Ze)}. \tag{15}$$

The input impedance of the amplifier $Z_{a1(2)}$ should be large, and the impedance on the transmission path $Z_{e1(2)}$ should be as small as possible to reduce the difference between the source ECG signal and the actual measured ECG signal. In this work, $Z_{e1(2)}$ contains the impedance of the conductive fiber trace and the impedance of the skin-electrode interface, and usually the skin-electrode impedance accounts for the majority of $Z_{e1(2)}$. In addition to the impedance characteristic of the conductive material, the impedance of the skin electrode interface can be influenced by the applied pressure and contact area. Therefore, by increasing the contact area of the ECG electrodes or making the ECG electrodes fit more closely to the body surface, the ECG signal with dry electrodes can be further improved. The ECG signal measured by the proposed system is also compared with that measured by the clinical standard lead-I ECG, and the result is shown in Fig. 13, showing the potential of the proposed system in medical applications. With regard to respiration, the function of the respiration transducer is validated by BIOPAC. The experimental verification shows good result with 98.74% accuracy in a test of 19 people.

Another emerging issue on the development of biosignal monitoring clothing is washing. In the current stage, the samples of the biosignal monitoring clothing were tested in 10 consecutive cycles of washing and drying. Washing was conducted in a washing machine, and the washing water temperature was approximately 40 °C. The washing time was 40 min per wash. A laundry bag was also used, but no detergent was used during washing. During drying, the clothing was lined dry in shade. In this experiment, a total of three samples of clothing were tested. After the complete washing test, the function of the samples was verified by comparing the measured result with that of the BIOPAC MP36 acquisition system. The result showed that the correctness of the ECG and respiratory signals measured using the washed samples was 99.94% and 98.90%, respectively. Therefore, the function of the washed samples was confirmed.

V. CONCLUSION

A complete smart clothing system, which provides the monitoring of lead-I ECG and respiratory signals, is proposed in this paper. The system primarily contains three main blocks, including biosignal monitoring clothing, a biosignal acquisition device, and a software platform on a remote smart device. The biosignal acquisition device with a supply voltage of 3.3 V primarily includes an ECG signal acquisition circuit, respiratory signal acquisition circuit, and microcontroller with a Bluetooth 5.2 module. The software platform is implemented on mobile device with an iOS platform to receive the data and provide real-time biosignal display, heart rate, respiration rate, and health information. The proposed QRS complex detection algorithm for heart rate acquisition is verified by the MIT-BIH database, and the performances, including Se, P+, and ERR, are 99.86%, 99.93%, and 0.19%, respectively. The function of the respiration transducer is validated by BIOPAC SS11LA airflow transducer, and the experimental verification shows good result with 98.74% accuracy in a test of 19 people. Using the proposed smart clothing system, the long-term biosignal monitoring for health care can be achieved.

ACKNOWLEDGMENT

The authors would like to thank the National Cheng Kung University Hospital and Tainan Hospital for their support of this work on clinical trial with IRB: B-ER-104-379.

REFERENCES

[1] World health organization. *Ageing and Health*. Accessed: Mar. 2021. [Online]. Available: https://www.who.int/news-room/fact-sheets/detail/ageing-and-health

[2] S.-Y. Lee, J.-H. Hong, C.-H. Hsieh, M.-C. Liang, S.-Y. C. Chien, and K.-H. Lin, "Low-power wireless ECG acquisition and classification system for body sensor networks," *IEEE J. Biomed. Health Informat.*, vol. 19, no. 1, pp. 236–246, Jan. 2015.

[3] G. B. Smith, D. R. Prytherch, P. Meredith, P. E. Schmidt, and P. I. Featherstone, *The Ability of the National Early Warning Score (NEWS) to Discriminate Patients at Risk of Early Cardiac Arrest, Unanticipated Intensive Care Unit Admission, and Death*. Accessed: Jun. 17, 2022. [Online]. Available: http://eprints.bournemouth.ac.uk/25324/26/Smith.%20NEWS.pdf

[4] The johns hopkins university. *Vital Signs (Body Temperature, Pulse Rate, Respiration Rate, Blood Pressure)*. Accessed: Mar. 2021. [Online]. Available: https://www.hopkinsmedicine.org/health/conditions-and-diseases/vital-signs-body-temperature-pulse-rate-respiration-rate-blood-pressure

[5] R. L. Lux, M. J. Burgess, R. F. Wyatt, A. K. Evans, G. M. Vincent, and J. A. Abildskov, "Clinically practical lead systems for improved electrocardiography: Comparison with precordial grids and conventional lead systems," *Circulation*, vol. 59, no. 2, pp. 356–363, Feb. 1979.

[6] NorthEast Monitoring Inc. *DR200/HE Digital Recorder for Holter and Event Recording Operator's Manual*. Accessed: Jun. 17, 2022. [Online]. Available: https://nemon.com/supportfiles/NEMM020-Rev-K_ENGLISH_DR200_Hookup.pdf

[7] M. Takano and A. Ueno, "Noncontact in-bed measurements of physiological and behavioral signals using an integrated fabric-sheet sensing scheme," *IEEE J. Biomed. Health Informat.*, vol. 23, no. 2, pp. 618–630, Mar. 2019.

[8] V. P. Rachim and W.-Y. Chung, "Wearable noncontact armband for mobile ECG monitoring system," *IEEE Trans. Biomed. Circuits Syst.*, vol. 10, no. 6, pp. 1112–1118, Dec. 2016.

[9] A. C. Myers, H. Huang, and Y. Zhu, "Wearable silver nanowire dry electrodes for electrophysiological sensing," *RSC Adv.*, vol. 5, no. 15, pp. 11627–11632, 2015.

[10] J.-Y. Baek, J.-H. An, J.-M. Choi, K.-S. Park, and S.-H. Lee, "Flexible polymeric dry electrodes for the long-term monitoring of ECG," *Sens. Actuators A, Phys.*, vol. 143, no. 2, pp. 423–429, May 2008.

[11] S. K. Kundu, S. Kumagai, and M. Sasaki, "A wearable capacitive sensor for monitoring human respiratory rate," *Jpn. J. Appl. Phys.*, vol. 20, no. 4, p. 04CL05, Apr. 2013.

[12] A. Boehm, X. Yu, W. Neu, S. Leonhardt, and D. Teichmann, "A novel 12-lead ECG T-shirt with active electrodes," *Electronics*, vol. 5, no. 4, p. 75, Nov. 2016.

[13] J. Kubicek, K. Fiedorova, D. Vilimek, M. Cerny, M. Penhaker, M. Janura, and J. Rosicky, "Recent trends, construction, and applications of smart textiles and clothing for monitoring of health activity: A comprehensive multidisciplinary review," *IEEE Rev. Biomed. Eng.*, vol. 15, pp. 36–60, 2022.

[14] M. Di Rienzo, E. Vaini, and P. Lombardi, "Development of a smart garment for the assessment of cardiac mechanical performance and other vital signs during sleep in microgravity," *Sens. Actuators A, Phys.*, vol. 274, no. 1, pp. 19–27, May 2018.

[15] Y. Koyama, M. Nishiyama, and K. Watanabe, "Smart textile using hetero-core optical fiber for heartbeat and respiration monitoring," *IEEE Sensors J.*, vol. 18, no. 15, pp. 6175–6180, Aug. 2018.

[16] Y. Bu, M. F. U. Hassan, and D. Lai, "The embedding of flexible conductive silver-coated electrodes into ECG monitoring garment for minimizing motion artefacts," *IEEE Sensors J.*, vol. 21, no. 13, pp. 14454–14465, Jul. 2021.

[17] R. E. Mason and I. Likar, "A new system of multiple-lead exercise electrocardiography," *Amer. Heart J.*, vol. 71, no. 2, pp. 196–205, Feb. 1966.

[18] M. Papouchado, P. R. Walker, M. A. James, and L. M. Clarke, "Fundamental differences between the standard 12-lead electrocardiograph and the modified (Mason-Likar) exercise lead system," *Eur. Heart J.*, vol. 8, no. 7, pp. 725–733, Jul. 1987.

[19] P. Kligfield, L. S. Gettes, J. J. Bailey, R. Childers, B. J. Deal, E. W. Hancock, G. V. Herpen, J. A. Kors, P. Macfarlane, D. M. Mirvis, O. Pahlm, P. Rautaharju, and G. S. Wagner, "Recommendations for the standardization and interpretation of the electrocardiogram: Part I: The electrocardiogram and its technology: A scientific statement from the American heart association electrocardiography and arrhythmias committee, council on clinical cardiology; the American college of cardiology foundation; and the heart rhythm society: Endorsed by the international society for computerized electrocardiology," *Circulation*, vol. 115, no. 10, pp. 1306–1324, Mar. 2007.

[20] W. J. Tompkins, *Biomedical Digital Signal Processing*. Hoboken, NJ, USA: Prentice-Hall, 2000.

[21] J. D. Bronzino, *The Biomedical Engineering Handbook*, 2nd ed. Boca Raton, FL, USA: CRC Press, 2000.

[22] S.-Y. Lee, P.-H. Su, K.-L. Huang, Y.-W. Hung, and J.-Y. Chen, "High-pass sigma–delta modulator with techniques of operational amplifier sharing and programmable feedforward coefficients for ECG signal acquisition," *IEEE Trans. Biomed. Circuits Syst.*, vol. 15, no. 3, pp. 443–453, Jun. 2021.

[23] G. M. Friesen, T. C. Jannett, M. A. Jadallah, S. L. Yates, S. R. Quint, and H. T. Nagle, "A comparison of the noise sensitivity of nine QRS detection algorithms," *IEEE Trans. Biomed. Eng.*, vol. 37, no. 1, pp. 85–98, Jan. 1990.

[24] D. B. Saadi, G. Tanev, M. Flintrup, A. Osmanagic, K. Egstrup, K. Hoppe, P. Jennum, J. L. Jeppesen, H. K. Iversen, and H. B. D. Sorensen, "Automatic real-time embedded QRS complex detection for a novel patch-type electrocardiogram recorder," *IEEE J. Translational Eng. Health Med.*, vol. 3, pp. 1–12, 2015.

[25] S. Yazdani and J.-M. Vesin, "A novel preprocessing tool to enhance ECG R: Wave extraction," in *Proc. Comput. Cardiol. Conf. (CinC)*, Sep. 2016, pp. 633–636.

[26] A. Kashani and S. S. Barold, "Significance of QRS complex duration in patients with heart failure," *J. Amer. College Cardiol.*, vol. 46, no. 12, pp. 2183–2192, Dec. 2005.

[27] A. Boggess and F. J. Narcowich, *A First course in Wavelets With Fourier Analysis*. Hoboken, NJ, USA: Wiley, 2009.

[28] H. Tanaka, K. Monahan, and D. Seals, "Age-predicted maximal heart rate revisited," *J. Amer. College Cardiol.*, vol. 37, no. 1, pp. 153–156, Jan. 2001.

[29] *MIT-BIH Arrhythmia Database*. Accessed: Jun. 17, 2022. [Online]. Available: https://www.physionet.org/content/mitdb/1.0.0/

[30] M. Malik, "Heart rate variability: Standards of measurement, physiological interpretation, and clinical use," *Circulation*, vol. 93, no. 5, pp. 1043–1065, Mar. 1996.

[31] L. Keytel, J. Goedecke, T. Noakes, H. Hiiloskorpi, R. Laukkanen, L. van der Merwe, and E. Lambert, "Prediction of energy expenditure from heart rate monitoring during submaximal exercise," *J. Sports Sci.*, vol. 23, no. 3, pp. 289–297, Mar. 2005.

[32] Contec Medical Systems Co. *MS400 ECG, Arrhythmia, IBP, Respiration Multi-Parameter Patient Simulator*. Accessed: Mar. 2021. [Online]. Available: https://contecmedical.en.made-in-china.com/product/tbIJfYUMqeRo/China-Ms400-ECG-Arrhythmia-IBP-Respiration-Multi-Parameter-Patient-Simulator.html

[33] BIOPAC System Inc. *Four Channel Data Acquisition System*. Accessed: Jun. 17, 2022. [Online]. Available: https://www.biopac.com/wp-content/uploads/MP36-MP46.pdf

[34] BIOPAC System Inc. *SS2L Electrode Lead Set*. Accessed: Jun. 17, 2022. [Online]. Available: https://www.biopac.com/wp-content/uploads/SS2L.pdf

[35] BIOPAC System Inc. *Medium-flow Pneumotach Transducer*. Accessed: Jun. 17, 2022. [Online]. Available: https://www.biopac.com/wp-content/uploads/Pneumotach-Handheld.pdf

[36] J. Pan and W. J. Tompkins, "A real-time QRS detection algorithm," *IEEE Trans. Biomed. Eng.*, vol. BE-32, no. 3, pp. 230–236, Mar. 1985.

[37] C.-L. Chen and C.-T. Chuang, "A QRS detection and R point recognition method for wearable single-lead ECG devices," *Sensors*, vol. 17, no. 9, pp. 1969–1987, Aug. 2017.

[38] Z. Hou, Y. Dong, J. Xiang, X. Li, and B. Yang, "A real-time QRS detection method based on phase portraits and box-scoring calculation," *IEEE Sensors J.*, vol. 18, no. 9, pp. 3694–3702, May 2018.

[39] A. Sharma, S. Patidar, A. Upadhyay, and U. Rajendra Acharya, "Accurate tunable-Q wavelet transform based method for QRS complex detection," *Comput. Electr. Eng.*, vol. 75, pp. 101–111, May 2019.

[40] S.-Y. Lee, P.-W. Huang, J.-R. Chiou, C. Tsou, Y.-Y. Liao, and J.-Y. Chen, "Electrocardiogram and phonocardiogram monitoring system for cardiac auscultation," *IEEE Trans. Biomed. Circuits Syst.*, vol. 13, no. 6, pp. 1471–1482, Dec. 2019.

[41] W. Cai and D. Hu, "QRS complex detection using novel deep learning neural networks," *IEEE Access*, vol. 8, pp. 97082–97089, 2020.

[42] J. Malik, E. Z. Soliman, and H.-T. Wu, "An adaptive QRS detection algorithm for ultra-long-term ECG recordings," *J. Electrocardiol.*, vol. 60, pp. 165–171, May 2020.

[43] GitHub. *YuCloth ECG QRS Detector*. Accessed: Nov. 2021. [Online]. Available: https://github.com/YuTecHealth/YuCloth_QRSDetector

[44] MATLAB Central File Exchange. *Complete Pan Tompkins Implementation ECG QRS detector*. Accessed: Jul. 2021. [Online]. Available: https://www.mathworks.com/matlabcentral/fileexchange/45840-complete-pan-tompkins-implementation-ecg-qrs-detector

[45] C. Ye, B. V. K. V. Kumar, and M. T. Coimbra, "An automatic subject-adaptable heartbeat classifier based on multiview learning," *IEEE J. Biomed. Health Informat.*, vol. 20, no. 6, pp. 1485–1492, Nov. 2016.
[46] S. Kiranyaz, T. Ince, and M. Gabbouj, "Real-time patient-specific ECG classification by 1-D convolutional neural networks," *IEEE Trans. Biomed. Eng.*, vol. 63, no. 3, pp. 664–675, Mar. 2016.
[47] X. Zhai and C. Tin, "Automated ECG classification using dual heartbeat coupling based on convolutional neural network," *IEEE Access*, vol. 6, pp. 27465–27472, 2018.
[48] C. Ye, B. V. K. V. Kumar, and M. T. Coimbra, "Heartbeat classification using morphological and dynamic features of ECG signals," *IEEE Trans. Biomed. Eng.*, vol. 59, no. 10, pp. 2930–2941, Oct. 2012.
[49] H. Zhu, Y. Zhao, Y. Pan, H. Xie, F. Wu, and R. Huan, "Robust heartbeat classification for wearable single-lead ECG via extreme gradient boosting," *Sensors*, vol. 21, no. 16, pp. 5290–5309, Aug. 2021.
[50] B. Taji, S. Shirmohammadi, V. Groza, and I. Batkin, "Impact of skin-electrode interface on electrocardiogram measurements using conductive textile electrodes," *IEEE Trans. Instrum. Meas.*, vol. 63, no. 6, pp. 1412–1422, Jun. 2014.

SHUENN-YUH LEE (Senior Member, IEEE) was born in Taichung, Taiwan, in 1966. He received the B.S. degree from the National Taiwan Ocean University, Keelung, Taiwan, in 1988, and the M.S. and Ph.D. degrees from the National Cheng Kung University, Tainan, Taiwan, in 1994 and 1999, respectively.

He is currently a Distinguished Professor with the Department of Electrical Engineering, National Cheng Kung University. His current research interests include the design of analog and mixed-signal integrated circuits, biomedical circuits and systems, artificial intelligence integrated circuits, low-power and low-voltage analog circuits, and RF front-end integrated circuits for wireless communications.

Dr. Lee is also a member of Circuits and Systems (CAS) Society, Solid-State Circuits Society, and Medicine and Biology Society of IEEE. He is also a member of IEICE. He served as the Technical Program Chair (TPC) for the 2014/2015 International Symposium on Bioelectronics & Bioinformatics (ISBB), and the 2015 Taiwan and Japan Conference on Circuits and Systems (TJCAS). He served as the General Co-Chair for the 2022 IEEE Biomedical Circuits and Systems Conference (BioCAS) and the Organization Chair for the 2022 IEEE Asia Solid-State Circuits Conference (ASSCC). From 2013 to 2016, he serves as the Chairperson for IEEE Solid-State Circuits Society Tainan Chapter. From 2016 to 2017, he serves as the Vice Chairperson for IEEE Tainan Section. Since 2016, he has been serving as the Associate Editor for IEEE Transaction on Biomedical Circuits and Systems.

YI-WEN HUNG (Student Member, IEEE) was born in Kaohsiung, Taiwan, in 1992. He received the B.S. degree from the National Cheng Kung University, Tainan, Taiwan, in 2015, where he is currently pursuing the Ph.D. degree with the Institute of Electrical Engineering.

His research interests include the design of wearable device for bio-signal monitoring, signal processing technology, machine learning algorithm, and bio-signal analysis.

PO-HAN SU (Graduate Student Member, IEEE) was born in Chiayi, Taiwan, in 1993. He received the B.S. degree from the National Cheng Kung University, Tainan, Taiwan, in 2015, where he is currently pursuing the Ph.D. degree with the Institute of Electrical Engineering.

His research interests include the design of analog integrated circuits, biomedical circuits and systems, and bio-signal processing algorithm.

I-PEI LEE was born in Tainan, Taiwan, in 1998. She is currently pursuing the B.S. degree with the School of Medicine, Kaohsiung Medical University, Kaohsiung, Taiwan.

Her current research interests include the cardiovascular diseases and applications of wearable medical devices.

JU-YI CHEN was born in Tainan, Taiwan, in 1974. He received the M.S. degree from Chang Gung University, Taoyuan City, Taiwan, in 1999, and the Ph.D. degree from the National Cheng Kung University, Tainan, in 2013.

Since 2021, he has been a Professor with the Department of Internal Medicine, National Cheng Kung University. His current research interests include the cardiovascular diseases, including arrhythmias, hypertension, arterial stiffness, and cardiac implantable electric devices.